Injury, Int. J. Care Injured 50 (2019) 648–656

Contents lists available at ScienceDirect

Injury

journal homepage: www.elsevier.com/locate/injury

Medial sustainable nail versus proximal femoral nail antirotation in treating AO/OTA 31-A2.3 fractures: Finite element analysis and biomechanical evaluation

Jiantao Li[a,1], Lin Han[b,1], Hao Zhang[a,1], Zhe Zhao[c], Xiuyun Su[a], Jianfeng Zhou[d], Chen Li[e], Peng Yin[f], Ming Hao[a], Kun Wang[a], Gaoxiang Xu[a], Lihai Zhang[a], Licheng Zhang[a,*], Peifu Tang[a,*]

[a] Department of Orthopaedics, Chinese PLA General Hospital, Beijing, China
[b] Graduate School of the Second Military Medical University, Shanghai, China
[c] Department of Orthopaedics, Beijing Tsinghua Changgung Hospital, School of Clinical Medicine, Tsinghua University, Beijing, China
[d] Department of Emergency, Chinese PLA General Hospital, Beijing, China
[e] Department of Orthopaedics, Tianjin Hospital, Tianjin, China
[f] Department of Orthopaedics, Beijing Chao-Yang Hospital, Beijing, China

ARTICLE INFO

Article history:
Accepted 12 February 2019

Keywords:
Finite element analysis
Biomechanics
Unstable intertrochanteric fractures
Intramedullary nail

ABSTRACT

Objectives: Using finite element analysis and biomechanical tests, the biomechanical behaviors of Medial Sustainable Nail (MSN) and Proximal Femoral Nail Antirotation (PFNA) were compared for the fixation of fracture type of AO/OTA 31-A2.3.
Methods: Finite element software Abaqus 6.14 was used to conduct axial loading of 2100 N and we analyzed the von Mises stress distribution and the model displacement of two implant models. Biomechanical tests were separately conducted in the axial stiffness test and axial cyclical loading test on a mechanical testing machine.
Results: The results indicate that von Mises stress of MSN was lower than that of PFNA, and the model displacement in the MSN group was lower than that in the PFNA group. In the axial stiffness tests, MSN group was stiffer than PFNA construct. With respect to the axial load to ultimate failure, the PFNA construct exhibited higher loads exceeding 4000 N while the MSN construct withstood 3313.8 ± 92.8 N. Specifically, F_{10mm} was 2178.6 ± 133.2 N of the MSN group and 1822.6 ± 93.1 N of the PFNA group (P = 0.001). Additionally, X_{2100N} was 9.8 ± 0.5 mm of the MSN group and 11.7 ± 0.7 mm of the PFNA group (P = 0.002). The MSN group exhibited superior performances in terms of the mean value of the vertical displacement, frontal rotation angle, and lateral rotation angle.
Conclusions: The results indicated that the MSN construct might exhibit a better biomechanical performance when compared with that of the PFNA in reducing displacement and anti-varus in fracture type of AO/OTA 31-A2.3.

Introduction

Intertrochanteric fractures are among the most common fractures associated with osteoporosis and account for 40–50% of all hip fractures [1–3]. Due to the growing population of elderly individuals in the world, these fractures are expected to gain clinical and economic importance in the future [4,5].

Reviews from Cochrane Database indicate that intramedullary nails are recommended for the treatment of unstable intertrochanteric fractures [6]. The use of intramedullary fixation increased recently due to its theoretical advantages and biomechanical superiority when compared with extramedullary fixation [7,8]. However, complication rates ranging to a maximum of 20.5% were reported with respect to the use of the intramedullary nail technique and especially in unstable fractures [9]. Various modifications and improvements of the intramedullary nails were examined in past years. However, complications persist.

* Corresponding authors at: Chinese PLA General Hospital, No. 28 Fuxing Road, Beijing 100853, China.
E-mail addresses: zhanglcheng218@126.com (L. Zhang), pftang301@163.com (P. Tang).
[1] The first three authors contributed equally to this work.

https://doi.org/10.1016/j.injury.2019.02.008
0020-1383/

Previous-generation intramedullary nails encountered frequent issues of screw backup after mobilization with weight bearing [10]. The complications of "Z" effect were occasionally observed in the second-generation nails characterized by the double hip screws [11]. In order to overcome this disadvantage of second-generation nails, PFNA, which corresponds to the third-generation nail, was designed and launched in the market. However, previous studies reported on the local complications including excessive sliding of the cephalic nail, proximal femur shorting, cut-out, and varus collapse [10,12].

The lack of the posterior-medial bone buttress at the junction of femoral shaft and neck creates an instability that leads to the varus-tendency or rotation of the proximal femoral fragment [13]. Additionally, the continuity of the posterior and medial cortex of the intertrochanteric region is treated as the keystone to mechanical stability for intertrochanteric fractures [14], and it is considered as essential to avoiding either failure modes.

Therefore, in the present study, we designed a new intramedullary nail based on the characteristics of the anatomy and biomechanics of proximal femur. The nail is termed as a Medial Sustainable Nail (MSN), and its aim involves reducing the complications of the unstable fracture types associated with the lack of posteromedial cortex. The MSN consists of a slightly angled cannulated nail shaft, cephalic nail, sustainable nail, and distal locking screw. A cephalic nail is composed of a sleeve and helical blade. A sustainable nail is equipped with a thread on the head that is firmly locked into the shaft nail, and the other end of it touches the sleeve slightly. The aforementioned features allow the reconstruction and support of the posterior and medial cortices. The cephalic nail, sustainable nail, and shaft nail form a triangular supporting system capable of performing the medial sustainable function and anti-rotation as well as resisting the varus deformity in theory (Fig. 1).

Therefore, the purpose of this study involved exploring the advantages and disadvantages of MSN when compared with PFNA by using finite element analysis and biomechanical tests. We hypothesized that MSN leads to increased biomechanical advantage when compared with those of PFNA in the fracture type corresponding to AO/OTA31-A2.3.

Fig. 1. Medial Sustainable Nail (MSN) that consists of a slightly angled cannulated nail shaft (purple arrow), cephalic nail (orange arrow), and sustainable nail (red arrow). The cephalic nail is composed of a sleeve (black arrow) and a helical blade (blue arrow). The sustainable nail is equipped with a thread on the head that is firmly locked into the shaft nail, and the other end of it touches the sleeve slightly. The distal part of the nail contains an oval hole for either dynamic or static locking purposes (For interpretation of the references to colour in this figure legend, the reader is referred to the web version of this article).

Materials and methods

Finite element analysis study

The geometric model of femur was employed from a three dimensional model of a left fourth-generation composite femur (MODEL3405#, Pacific Research Laboratories, Vashon, WA). Subsequently we constructed the fracture model in 3-matic (Materialise, Belgian) to simulate AO/OTA type 31-A2.3 fracture [15] according to the fracture lines described by Fensky F et al. [16]. The first simulated fracture line was made 1 cm below the greater trochanter through the intertrochanteric ridge to the bottom of the lesser trochanter with an angle of 20° with respect to the axis of the femur. The second fracture line was created from the tip of the greater trochanter towards the intersection of the first osteotomy and the top of the lesser trochanter, which was removed (Fig. 2 A–B).

According to the manufacturer-provided engineering drawing, the 3D models of intramedullary nails (PFNA and MSN) were modeled by using the Unigraphics NX 8.5 software (Siemens PLM Software). Assemblage of the internal fixations and bones was accomplished in 3-matic. All the models were meshed by using the software HyperMesh 11.0 (Altair Engineering, Inc, USA).

The assembled three-dimensional models were imported into ABAQUS (Simulia, France) to generate the finite element models. The implants were composed of titanium. The synthetic bone was assumed as homogeneous and isotropic with linear elastic properties as reported by the manufacturer and previous studies [17–19]. The mechanical properties of the implant and bone materials are shown on the Table 1.

Frictional contact interactions were assumed between the different parts of the models. The interfaces between bone and internal fixations were simulated by contact pairs with a friction factor of 0.3 and the friction coefficients for bone-bone interaction was 0.46 [20]. The interface of sustainable nail and nail shaft of MSN was set as tie constraints. All nodes on the surface of distal femur were constrained with 0° of freedom. This study simulated the forces performing on the hip during walking. In this model, the femoral head was subjected to a load of 2100 N through 7 steps, which included 300 N, 600 N, 900 N, 1200 N, 1500 N, 1800 N and 2100 N. The net force was applied to the femoral head at 10° laterally in the coronal plane and 9° posteriorly on the sagittal plane [21].

The analysis was performed by using finite element software Abaqus 6.14 (Simulia Corp., USA). The von Mises stress distribution and the model displacement were used to compare the effect of fixation constructs. The model principal strains of proximal fragment was used to capture the mechanical factors in this study.

Biomechanical tests

Preparation and osteotomy

Fourteen large left fourth-generation composite femurs (Model 3406; Pacific Research Laboratories, Vashon, WA) were randomly assigned into two groups, namely the MSN group, and PFNA group (10 in axial stiffness tests and 4 in axial cyclical loading tests). Before osteotomy, an intramedullary nail was inserted into the composite femur. Furthermore, TAD was controlled within a satisfactory position of 25 mm [22].

Additionally, we designed the osteotomy molds in the 3-matic software which matched the femur properly (Fig. 2 C–D). The osteotomy molds were obtained by using a 3D printer (OBJET

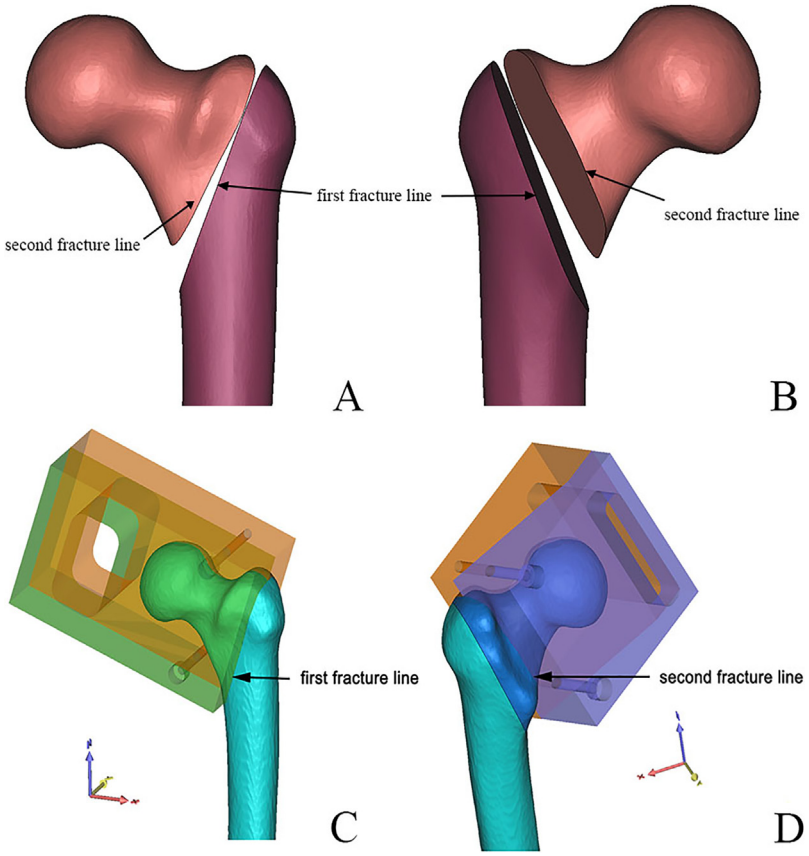

Fig. 2. (A–B) AO/OTA type 31-A2.3 fracture model was created in the software of 3-matic. (C–D) Materialise 3-matic software was used to design intertrochanteric fracture osteotomy molds according to the fracture line.

Table 1
Mechanical features of the implant and bone.

Material	Elastic modulus (N/mm^2)	Poisson's ratio
Titanium(Ti6Al4V)	113.8 GPa	0.34
Cancellous bone	77.4 MPa	0.3
Cortical bone	12.4 GPa	0.3

EDEN260 V, Stratasys Ltd, Rehovot, Israel). After assembling the osteotomy molds and the femur, we used a horizontal bandsaw machine (Yandangshan Machine Tool Co., Ltd, Zhejiang Province, China) to obtain the flat margin of the fracture line, and finally the AO31-A2.3 fracture models [15] were created as per Fensky F et al. [16].

Fixation

After osteotomy, the implant fixation was operated again. The distal femoral condyles were resected at 30 cm distance from the proximal tip of the greater trochanter. Subsequently, 10 cm length of the distal diaphysis was embedded into polymethylmethacrylate in steel cylinders. Samples were loaded axially with the femurs positioned at 10° of adduction and 9° of posterior flexion to simulate a single-leg stance [23,24]. Two points were marked at 0.5 mm distal from the cutting plane of fragments on each side. These points were used to measure changes in the angle alongside the gap at frontal view. Mechanical tests (Fig. 3A) were conducted for an axial static loading test, and an axial cyclical loading test was conducted separately on an Instron mechanical testing machine (ElectroPuls E10000, Instron, Grove City, USA).

Axial stiffness tests

The vertical loads were incrementally applied to the femurs at a speed of 6 mm/s commencing from 0 N until the failure of the construct. The loads were transmitted through a custom-made hemispherical steel bowl acting on the top of the femoral head. Failures were defined as either corresponding to cutout/cut-through of the implant, implant failure, fracture of the femoral neck or shaft, reaching 10 mm of axial displacement, or a 30% load drop corresponding to an irreversible negative slope observed at the load–displacement curve. The peak of the curve was defined as the ultimate failure load, and the linear slope of the curve was defined as the stiffness [25]. A Nikon camera was used to capture all the experimental procedures at a rate of two photos per second.

Other primary measurements included F_{10mm} (force at 10 mm vertical displacement), X_{2100N} (displacement at a load of 2100 N), and α_{2100N} (frontal rotational angle of two fragments at a load of 2100 N) (Fig. 3B).

With respect to the safety of the tests, we stopped the tests when the maximal load reached 4000 N without any failures.

Axial cyclical loading tests

Cyclical loading tests were applied to the specimens for 10,000 times at a frequency of 2 Hz. The load changed from 210 N to 2100 N and subsequently back to 210 N in a sinusoidal manner. Failure modes were defined as described above in axial stiffness tests. In the same manner, videos were recorded by using the Nikon camera for 10 s at the cyclical numbers corresponding to 50, 1,000, 2000,

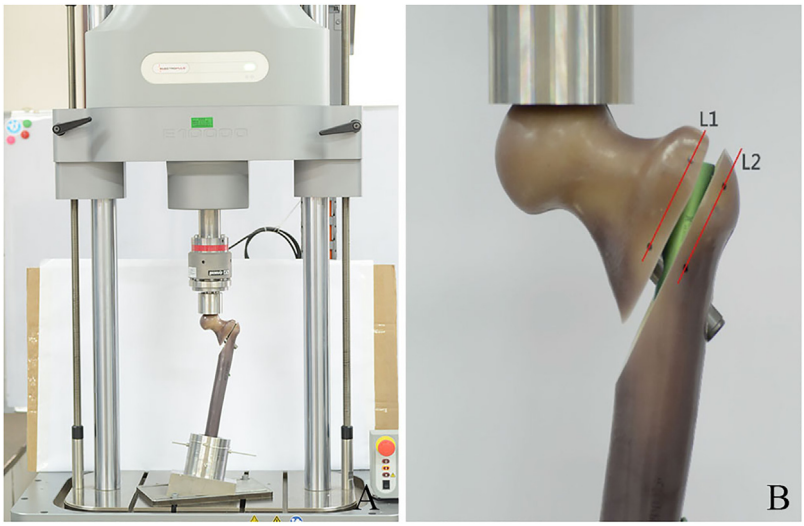

Fig. 3. (A) Illustration of the mechanical test setup and the osteotomy model of AO/OTA 31-A2.3 fracture. (B) Two lines are used to calculate the frontal rotation angle.

and 4000. This was followed by at every 2000 cycles up to 10,000 cycles to simulate the postoperative loading numbers during the first 4–6 weeks after fixation [26]. Subsequently, the mean value of the vertical displacement, frontal rotation angle, and lateral rotation angle were calculated from the values obtained during the periodic 10 cycles [27]. If the specimens survived after 10,000 cycles, then testing was performed continually till failure and the total number of cycles was recorded.

CT scans

CT scans (SOMATOM Sensation Open, Siemens AG, Erlangen, Germany) were performed before and after the biomechanical tests. Subsequently, CT data was imported into Mimics 16.0 Software and resliced functions were used to create new coronal planes through three points (the first point was located on the tip of the helical blade; the second point was on the proximal circle center of the shaft nail; and the third point was on the most remote circular center of the shaft nail). The changes in the femur and nails were easily discovered by comparing the CT data before and after the experiment.

Statistical analysis

Data analyses were performed by using SPSS (version 18.0, SPSS Inc., Chicago, Illinois). All tests were performed under uniform conditions. Mechanical parameters were compared by using the Student's t-test. Mechanical parameters of each group were presented as mean ± standard deviation (X ± S). The level of significance was set at $p < 0.05$.

Results

The number of elements in the nodes and models are shown in the Tables 2 and 3.

The von Mises stress distribution and the model displacement

The von Mises stress patterns of the increasing loads in two implant groups are shown in Fig. 4 A–B. The MSN indicated lower stress values when compared with those of PFNA. The stress value of the cephalic nail of MSN was lower than that of PFNA. Stresses of MSN cephalic nail appeared as concentrated on the junction of the sleeve and the helical blade while the cephalic nail of the PFNA indicated the stress concentration on the interaction between the nail shaft and the helical blade.

The model displacement patterns of the increasing loads in two implant groups are shown in Fig. 4 C. The values of model displacement in MSN group were lower than those in the PFNA group.

Maximum principal strains in proximal fragment

Contour plots showing maximum principal strains in proximal fragment bone in a cross-section through the major line were shown in Fig. 5 for the two nails. This figure is based on the assumption that failure of screw cut-out from the head is likely to occur due to high strains in the weak region of the proximal bone fragment [28]. Areas characterized by strains larger than a cut-off value of 0.9% maximum principal strain were assigned orange color to emphasize the regions where the bone was susceptible to yielding in accordance with recently published data [29]. Volume of cancellous bone in the proximal fragment with maximum principal strains above yield strain value of 0.9% was shown in Fig. 5.

Axial stiffness tests

A turning point was observed in every load–displacement curve of MSN group, and this divided the curve into two stages with different slopes indicating the changing stiffness of the constructs

Table 2
Number of nodes and elements in the Medial Sustainable Nail construct.

	Femur	Cephalic nail	Sleeve	Sustainable nail	Nail shaft	Distal locking screw
Elements	276279	20922	480	6455	38075	16173
Nodes	52564	34917	756	10326	61688	24771
Mesh size(mm)	Maximum: 3; minimum: 0.5	1.2	2.7	1.1	2.0	1.0

Note: MSN = Medial Sustainable Nail.

Table 3
Number of nodes and elements in the Proximal Femoral Nail Antirotation construct.

	Femur	Cephalic nail	Nail shaft	Distal locking screw
Elements	335429	17744	38577	16173
Nodes	63159	28651	61456	24771
Mesh size(mm)	Maximum: 3; minimum: 0.5	1.5	2.0	1.0

Note: PFNA = Proximal Femoral Nail Antirotation.

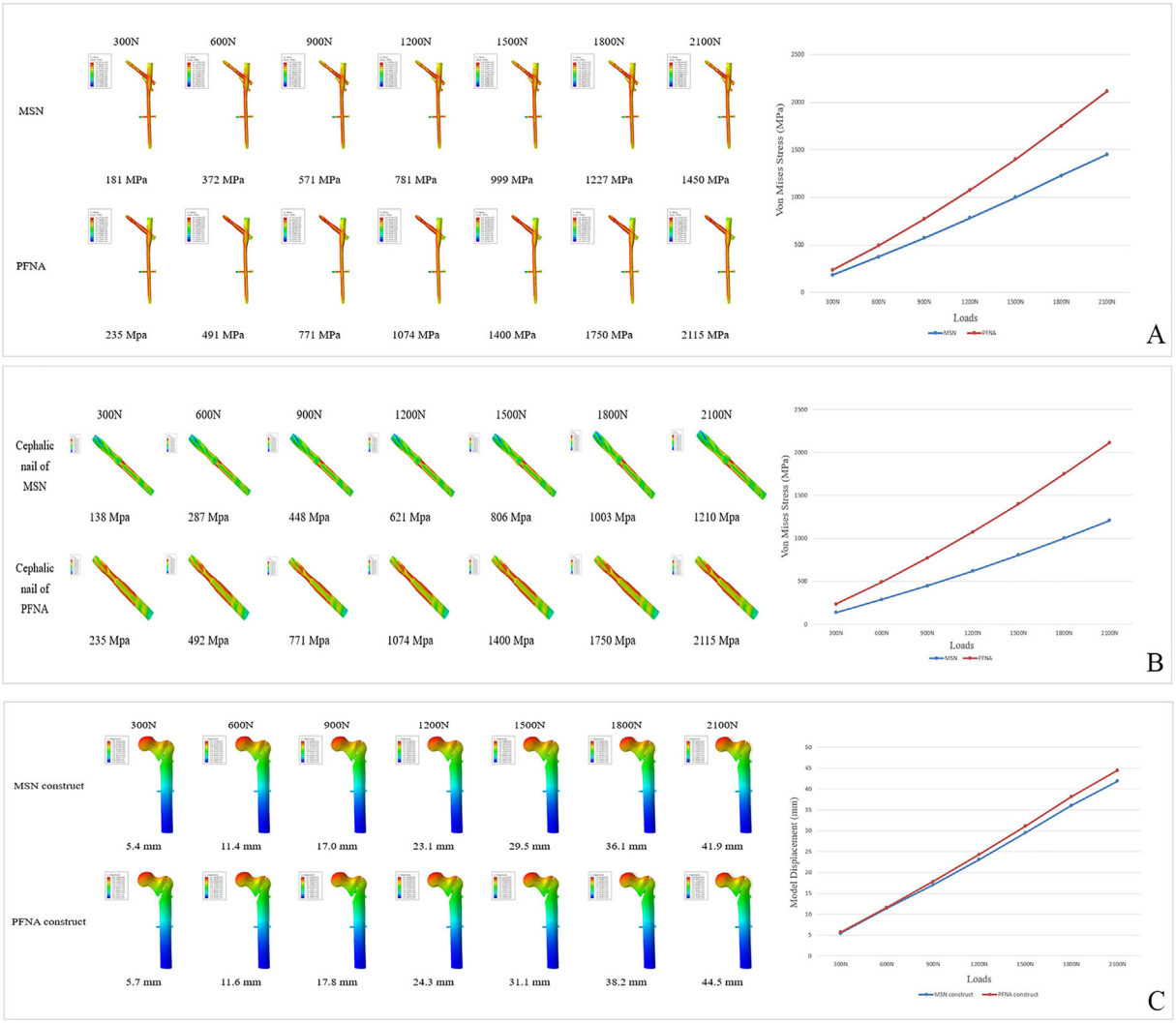

Fig. 4. Contour plots of von Mises stress in two implant groups (A), the cephalic nails (B) and the model displacements (C) with respect to increasing loads.

(Fig. 6). This was termed as MSN-Stage 1 and MSN-Stage 2. The MSN construct resulted in a axial stiffness of 162.6 ± 10.1 N/mm (Stage 1) (P = 0.223) and 214.2 ± 19.3 N/mm (Stage 2) (P = 0.013) when compared with PFNA construct (175.4 ± 19.2 N/mm). The load at the turning point was 397.6 ± 177.9 N, and the displacement was 2.8 ± 1.2 mm. With respect to the axial load to ultimate failure, the PFNA construct exhibited higher loads exceeding 4000 N while the MSN construct withstood 3313.8 ± 92.8 N. Specifically, F_{10mm} was 2178.6 ± 133.2 N of the MSN group and 1822.6 ± 93.1 N of the PFNA group (P = 0.001). Additionally, X_{2100N} was 9.8 ± 0.5 mm of the MSN group and 11.7 ± 0.7 mm of the PFNA group (P = 0.002). Furthermore, α_{2100N} was 9.4 ± 4.5° of the MSN group and 13.8 ± 6.8° of the PFNA group (P = 0.223).

The CT data indicated the occurrence of different bending locations in the two groups. The bending point was located at the junction of the helical blade and locking sleeve in the MSN group. In the PFNA group, the location corresponded to the intersection of the blade and nail. (Fig. 7)

Cyclic axial loading tests

With respect to axial cycles to failure, the PFNA construct exhibited a higher axial cyclic deformation limit with cycles corresponding to 138,801 and 64,523 when compared with the MSN construct with 58,621 and 56,000 cycles. With respect to the failure modes, both MSN and PFNA constructs exhibited rupture of the intramedullary nail in conjunction with the lateral wall of greater trochanter split (Fig. 8). The mean values of the vertical displacement, frontal rotation angle, and lateral rotation angle are shown in Fig. 9.

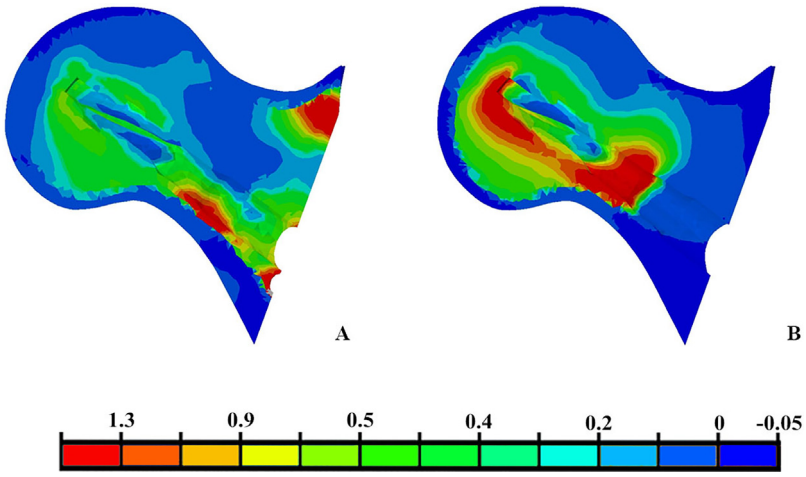

Fig. 5. Diagrams showing the maximum principal strains plotted in percent with a yield strain cut-off value of 0.9%. Orange regions have strains above 0.9% and are at higher risk in blade cut-out. (A) MSN model. (B) PFNA model.

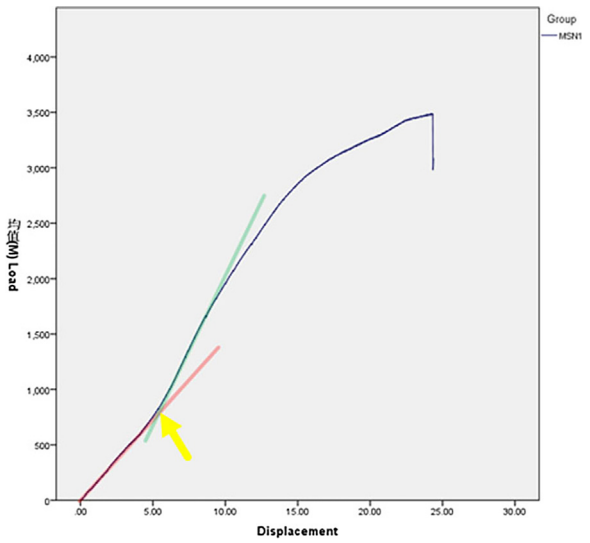

Fig. 6. A turning point (yellow arrow pointed) appears in the load–displacement curve of MSN group and divides the curve into two stages with different slopes (For interpretation of the references to colour in this figure legend, the reader is referred to the web version of this article).

Discussion

In the present study, we investigated the biomechanical properties of Medial Sustainable Nail (MSN) and Proximal Femoral Nail Antirotation (PFNA) for unstable intertrochanteric fractures by using finite element analysis and biomechanical tests. In order to examine the problem, we conducted this research and the results indicated that MSN exhibited mechanical reliability and advantages of anti-varus function when compared with PFNA construct in the AO/OTA type 31-A2.3 fracture models. The study supports the concept that the reconstruction of the medial sustainable support is critical in maintaining the posterior and medial cortices positions while treating unstable intertrochanteric fractures.

As shown in Fig. 4A, the stress distribution was similar for both the implants. However, the maximal stress in MSN was lower than that in PFNA, and the sustainable nail undertook part of the stress, thereby indicating good dispersion. As shown in Fig. 4B, the stress of MSN cephalic nail appeared as concentrated in the junction of the sleeve and the helical blade while the cephalic nail of the PFNA indicated a concentration on the interaction between the nail shaft and the helical blade, thereby implying that the lever arm in the MSN construct was shorter than that in PFNA construct. The von Mises stresses of PFNA exceeded the yield stress in the earlier subjecting load process, which means that MSN had more mechanical superiority. Both the implants exceeded the yield stress in the finite element analysis, however, our aim was to examine trends rather than absolute values. We relied on the maximum principal strains and a corresponding yield strain to evaluate the risk of blade cut-out. The stability of the screws within the head depends on an adequate anchorage in bone structure. It is necessary to avoid straining the bone beyond its yield point. Fig. 5 showed the bone structure susceptible to yielding in the femoral head region, which indicated that the MSN was less likely to be involved in cut-out than PFNA and was more stable. The CT data of the axial tests confirmed that there were differences in the concentrations of the cephalic nails, and the bending area was in accordance with the localized regions (Fig. 7). The displacement of the finite element analysis indicated that the MSN construct was more stable when compared with the PFA construct. Additionally, the values of F_{10mm} and X_{2100N} in the biomechanical tests also indicated the advantage of MSN. In the biomechanical tests, a turning point was observed in the load–displacement curves of the MSN constructs. After the turning point, the stiffness of the MSN construct exceeded that of the PFNA. The appearance of the turning point was termed as the secondary stabilization phenomenon, and it was formed by contact between the top of sustainable nail with the cephalic nail or the fragment of medial cortices. An increase in the stiffness is associated with earlier occurrences of the feasibility of secondary stability. Both the structures continuously bore the axial compression continuously and were in tight contact with each other leading to the formation of the triangle structure of the nail formed and an increase in the stiffness. As shown in Fig. 9, values of vertical displacement, frontal rotation angle, and lateral rotation angle also indicated improvements in the biomechanical performance of the MSN group in the axial cyclical loading tests. The aforementioned results indicated that triangular supporting system formed by the MSN possessed a sustainable function, exhibited better anti-bending and anti-rotation properties, resisted the varus deformity, and implemented the secondary stabilization earlier.

The 31-A2.3 fracture classification was characterized by the posterior cortex of the intertrochanteric crest being comminuted with lesser trochanteric detachment in which the major fracture

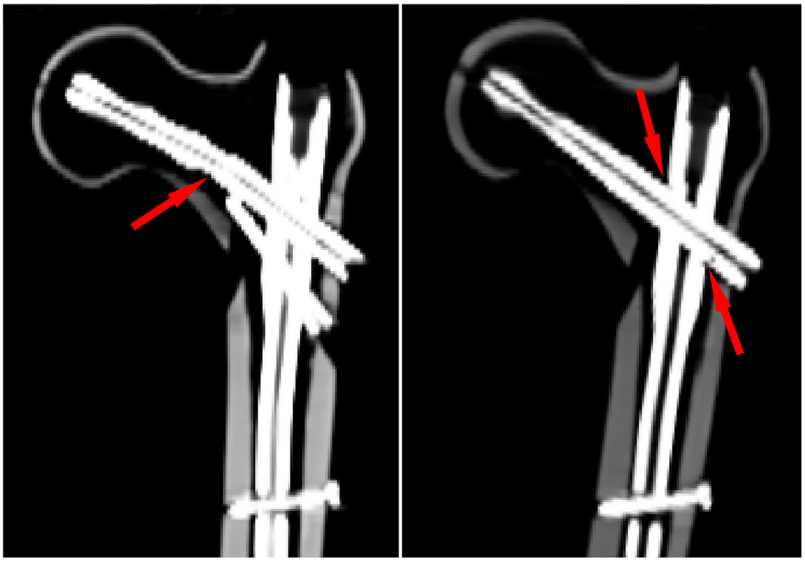

Fig. 7. The CT data indicates the different bending locations in two groups. The MSN group indicates the bending point located at the junction of helical blade and locking sleeve. In the PFNA group, the location corresponds to the intersection of the blade and nail.

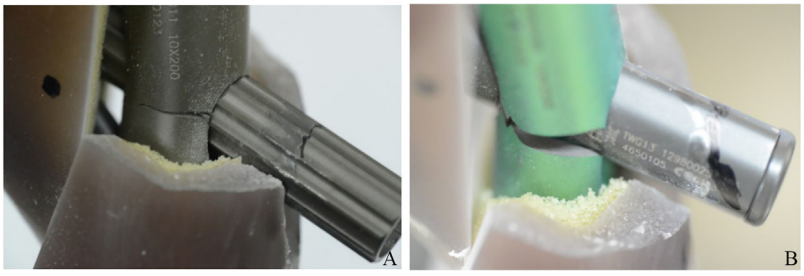

Fig. 8. Both MSN and PFNA constructs exhibit rupture of the intramedullary nail in conjunction with the lateral wall exhibiting a higher trochanter split.

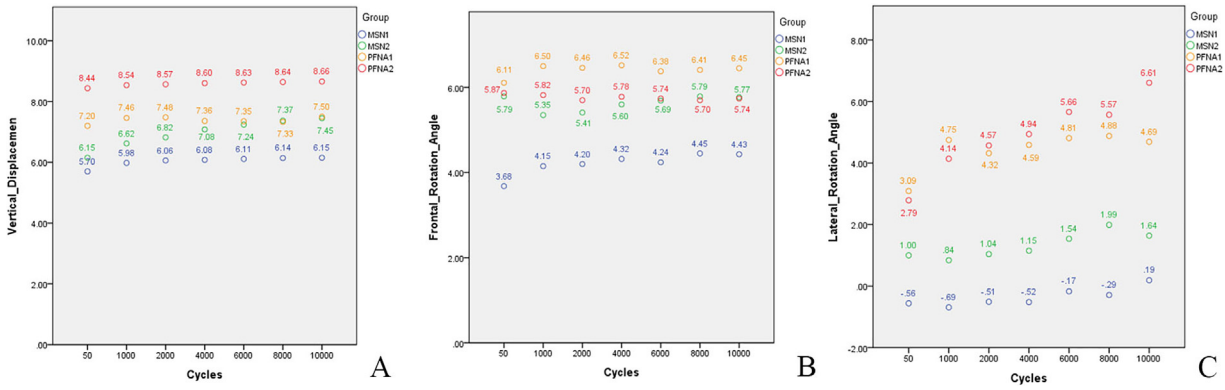

Fig. 9. Mean values of the vertical displacement (A), frontal rotation angle (B), and lateral rotation angle (C) indicating the higher stability of the MSN group when compared with that of the PFNA group.

line extends more than 1 cm below the lower trochanter. The lack of the medial buttress for the PFNA increases the risk of varus in this unstable fracture, and this leads to increased vertical displacement of the proximal fractures [30–32]. The sustainable nail of the MSN includes the advantage of reconstructing the medial cortices and can be used in the unstable fractures, such as A2.3, and secures the fracture block in the right place till the fracture union occurs.

The finite element analysis results of PFNA were similar to those in previous studies [20,30,33], and this indicated that the methods used in the study are reliable. Additionally, the advantages exhibited by the MSN with respect to the finite element analysis was verified by the biomechanical tests. The biomechanical values in the present study were similar to the values recorded in previous studies involving the cephalomedullary nail. Axial stiffness for the present study exhibited good agreement with that obtained in the study by Eberle [34]. Load-to-failure values for the present study was 3306N of the MSN corresponding to 5 times body weight and more than 4000N of the PFNA. Conversely, previous studies recorded average values ranging from 2035N to 3780N [35–39]. In

the cyclic axial loading tests, the primary failure mode with both the groups corresponded to a rupture of intramedullary nail along the lateral wall exhibiting a higher trochanter split (Fig. 8). Knobe et al. [39] obtained a similar failure mode in the PFNA construct, thereby indicating the principle failure mechanism with PFNA. The intramedullary shaft nail prevented the lateralization of the head-neck fragment by directly blocking the unstable fracture types and tended to varus collapse [40]. Given the medial support advantages of MSN, the varus collapse of the MSN group was lower than that of PFNA group, and the contribution of the stress contributed to the PFNA shaft was higher. Finally, the gap on the PFNA was evident.

The present study includes the following innovations: (1) Individual customization and rapid prototyping technology were used to establish fracture lines. This technique significantly reduces the differences in fracture patterns and guarantees consistency prior to biomechanical experiments. (2) The CT data was selected to detect tiny changes in the study. Most previous studies examined X-ray films as opposed to CT scans to analyze changes after experiments [25,27,41,42], and this is less accurate. Specifically, CT data includes numerous advantages in terms of multi-dimensional perspectives and positioning accuracy. (3) An implant-femur specimen was often used in different types of tests to save materials and costs [24,41,43–45]. However, in the present study, axial stiffness tests and cyclical loading tests were performed separately to guarantee the accuracy of the data.

To the best of the authors' knowledge, this is the first study to investigate the biomechanical advantages of the new designed MSN when compared with those of PFNA for unstable inter-trochanteric fractures by using a 3D-printing-osteotomy mold. We introduced a new concept to design the intramedullary nail and demonstrated its advantages. Nevertheless, the customized tooling, 3D printing technology, and individual tests used in the present study entailed higher costs. Additionally, the number of samples was relatively small. Furthermore, a future study should consider a few modifications in the MSN.

Conclusions

The results of this study indicated that the MSN construct might exhibit a better biomechanical performance when compared with that of the PFNA in reducing displacement and anti-varus. Specifically, MSN may be effective and feasible when it is used for unstable intertrochanteric fractures by reconstructing the medial sustainable support.

Conflicts of interest

There are no conflicts of interest of all authors.

Funding statement

This work was supported by the capital health research and development of special grants (2016-1-5012).

References

[1] Herman A, Landau Y, Gutman G, Ougortsin V, Chechick A, Shazar N. Radiological evaluation of intertrochanteric fracture fixation by the proximal femoral nail. Injury 2012;43(6):856–63.
[2] Bergström U, Jonsson H, Gustafson Y, Pettersson U, Stenlund H, Svensson O. The hip fracture incidence curve is shifting to the right. Acta Orthop 2009;80(5):520–4.
[3] Weiser L, Ruppel A, Nüchtern J, Sellenschloh K, Zeichen J, Püschel K, Morlock M, Lehmann W. Extra- vs. intramedullary treatment of pertrochanteric fractures: a biomechanical in vitro study comparing dynamic hip screw and intramedullary nail. Arch Orthop Trauma Surg 2015;135(8):1101–6.
[4] White S, Griffiths R. Projected incidence of proximal femoral fracture in England: a report from the NHS Hip Fracture Anaesthesia Network (HIPFAN). Injury 2011;42(11):1230–3.
[5] Kannus P, Parkkari J, Sievanen H, Heinonen A, Vuori I, Jarvinen M. Epidemiology of hip fractures. Bone 1996;18(1 Suppl):57s–63s.
[6] Parker MJ, Handoll HHG. Gamma and other cephalocondylic intramedullary nails versus extramedullary implants for extracapsular hip fractures in adults. Cochrane Database Syst Rev 2010(9).
[7] Anglen JO, Weinstein JN. Nail or plate fixation of intertrochanteric hip fractures: changing pattern of practice. A review of the American Board of Orthopaedic Surgery Database. J Bone Joint Surg Am 2008;90(4):700–7.
[8] Curtis MJ, Jinnah RH, Wilson V, Cunningham BW. Proximal femoral fractures: a biomechanical study to compare intramedullary and extramedullary fixation. Injury 1994;25(2):99–104.
[9] Liu W, Zhou D, Liu F, Weaver MJ, Vrahas MS. Mechanical complications of intertrochanteric hip fractures treated with trochanteric femoral nails. J Trauma Acute Care Surg 2013;75(2):304–10.
[10] Seyhan M, Turkmen I, Unay K, Ozkut A. Do PFNA devices and Intertan nails both have the same effects in the treatment of trochanteric fractures? A prospective clinical study. J Orthop Sci 2015;20(6):1053–61.
[11] Pires RE, Santana [44_TD$DIFF][38_TD$DIFF]Jr. EO, Santos LE, Giordano V, Balbachevsky D, Dos Reis FB. Failure of fixation of trochanteric femur fractures: clinical recommendations for avoiding Z-effect and reverse Z-effect type complications. Patient Saf Surg 2011;5:17.
[12] Lobo-Escolar A, Joven E, Iglesias D, Herrera A. Predictive factors for cutting-out in femoral intramedullary nailing. Injury 2010;41(12):1312–6.
[13] Sommers M, Roth C, Hall H, Kam B, Ehmke L, Krieg J, Madey S, Bottlang M. A laboratory model to evaluate cutout resistance of implants for pertrochanteric fracture fixation. J Orthop Trauma 2004;18(6):361–8.
[14] Apel D, Patwardhan A, Pinzur M, Dobozi W. Axial loading studies of unstable intertrochanteric fractures of the femur. Clin Orthop Relat Res 1989;156–64.
[15] Marsh JL, Slongo TF, Agel J, Broderick JS, Creevey W, DeCoster TA, Prokuski L, Sirkin MS, Ziran B, Henley B, Audige L. Fracture and dislocation classification compendium - 2007: Orthopaedic Trauma Association classification, database and outcomes committee. J Orthop Trauma 2007;21(10 Suppl):S1–133.
[16] Fensky F, Nüchtern J, Kolb J, Huber S, Rupprecht M, Jauch S, Sellenschloh K, Püschel K, Morlock M, Rueger J, Lehmann W. Cement augmentation of the proximal femoral nail antirotation for the treatment of osteoporotic pertrochanteric fractures–a biomechanical cadaver study. Injury 2013;44(6):802–7.
[17] Heiner A. Structural properties of fourth-generation composite femurs and tibias. J Biomech 2008;41(15):3282–4.
[18] Grassi L, Väänänen S, Amin Yavari S, Weinans H, Jurvelin J, Zadpoor A, et al. Experimental validation of finite element model for proximal composite femur using optical measurements. J Mech Behav Biomed Mater 2013;21:86–94.
[19] Gardner M, Chong A, Pollock A, Wooley P. Mechanical evaluation of large-size fourth-generation composite femur and tibia models. Ann Biomed Eng 2010;38(3):613–20.
[20] Eberle S, Gerber C, von Oldenburg G, Högel F, Augat P. A biomechanical evaluation of orthopaedic implants for hip fractures by finite element analysis and in-vitro tests. Proc Inst Mech Eng H 2010;224(10):1141–52.
[21] Nüchtern J, Ruecker A, Sellenschloh K, Rupprecht M, Püschel K, Rueger J, Morlock M, Lehmann W. Malpositioning of the lag-screws by one- or two-screw nailing systems for pertrochanteric femoral fractures: a biomechanical comparison of Gamma3 and Intertan. J Orthop Trauma 2014.
[22] Baumgaertner MR, Curtin SL, Lindskog DM, Keggi JM. The value of the tip-apex distance in predicting failure of fixation of peritrochanteric fractures of the hip. J Bone Joint Surg Am 1995;77(7):1058–64.
[23] Hunt S, Martin R, Woolridge B. Fatigue testing of a new locking plate for hip fractures. J Med Biol Eng 2012;32(2):117–22.
[24] Nuchtern JV, Ruecker AH, Sellenschloh K, Rupprecht M, Puschel K, Rueger JM, Morlock MM, Lehmann W. Malpositioning of the lag-screws by one- or two-screw nailing systems for pertrochanteric femoral fractures: a biomechanical comparison of Gamma3 and Intertan. J Orthop Trauma 2014.
[25] Knobe M, Gradl G, Maier KJ, Drescher W, Jansen-Troy A, Prescher A, Knechtel T, Antony P, Pape HC. Rotationally stable screw-anchor versus sliding hip screw plate systems in stable trochanteric femur fractures: a biomechanical evaluation. J Orthop Trauma 2013;27(6):e127–36.
[26] Kubiak EN, Bong M, Park SS, Kummer F, Egol K, Koval KJ. Intramedullary fixation of unstable intertrochanteric hip fractures: one or two lag screws. J Orthop Trauma 2004;18(1):12–7.
[27] Konstantinidis L, Papaioannou C, Hirschmuller A, Pavlidis T, Schroeter S, Sudkamp NP, et al. Intramedullary nailing of trochanteric fractures: central or caudal positioning of the load carrier? A biomechanical comparative study on cadaver bones. Injury 2013;44(6):784–90.
[28] Goffin JM, Pankaj P, Simpson AH. The importance of lag screw position for the stabilization of trochanteric fractures with a sliding hip screw: a subject-specific finite element study. J Orthop Res 2013;31(4):596–600.
[29] Goffin J, Pankaj P, Simpson A, Seil R, Gerich T. Does bone compaction around the helical blade of a proximal femoral nail anti-rotation (PFNA) decrease the risk of cut-out? A subject-specific computational study. Bone Joint Res 2013;2(5):79–83.
[30] Goffin J, Pankaj P, Simpson A. A computational study on the effect of fracture intrusion distance in three- and four-part trochanteric fractures treated with Gamma nail and sliding hip screw. J Orthop Res 2014;32(1):39–45.
[31] Hoffmann S, Paetzold R, Stephan D, Puschel K, Buehren V, Augat P. Biomechanical evaluation of interlocking lag screw design in intramedullary nailing of unstable pertrochanteric fractures. J Orthop Trauma 2013;27(9):483–90.

[32] Bonnaire F, Lein T, Bula P. [Trochanteric femoral fractures: anatomy, biomechanics and choice of implants]. Unfallchirurg 2011;114(6):491–500.
[33] Yuan G, Shen Y, Chen B, Zhang W. Biomechanical comparison of internal fixations in osteoporotic intertrochanteric fracture. A finite element analysis. Saudi Med J 2012;33(7):732–9.
[34] Eberle S, Gabel J, Hungerer S, Hoffmann S, Patzold R, Augat P, et al. Auxiliary locking plate improves fracture stability and healing in intertrochanteric fractures fixated by intramedullary nail. Clin Biomech (Bristol, Avon) 2012;27(10):1006–10.
[35] Kuzyk P, Zdero R, Shah S, Olsen M, Waddell J, Schemitsch E. Femoral head lag screw position for cephalomedullary nails: a biomechanical analysis. J Orthop Trauma 2012;26(7):414–21.
[36] Mahomed N, Harrington I, Kellam J, Maistrelli G, Hearn T, Vroemen J. Biomechanical analysis of the gamma nail and sliding hip screw. Clin Orthop Relat Res 1994;280–8.
[37] Heiney J, Battula S, Njus G, Ruble C, Vrabec G. Biomechanical comparison of three second-generation reconstruction nails in an unstable subtrochanteric femur fracture model. Proc Inst Mech Eng H 2008;222(6):959–66.
[38] Haynes R, Pöll R, Miles A, Weston R. Failure of femoral head fixation: a cadaveric analysis of lag screw cut-out with the gamma locking nail and AO dynamic hip screw. Injury 1997;28(5-6):337–41.
[39] Knobe M, Nagel P, Maier K, Gradl G, Buecking B, Sönmez T, Modabber A, Prescher A, Pape H. Rotationally stable screw-anchor with locked trochanteric stabilizing plate versus proximal femoral nail antirotation in the treatment of AO/OTA 31A2.2 fracture: a biomechanical evaluation. J Orthop Trauma 2016;30(1):e12–18.
[40] Hardy D, Descamps P, Krallis P, Fabeck L, Smets P, Bertens C, et al. Use of an intramedullary hip-screw compared with a compression hip-screw with a plate for intertrochanteric femoral fractures. A prospective, randomized study of one hundred patients. J Bone Joint Surg Am 1998;80(5):618–30.
[41] Takemoto RC, Lekic N, Schwarzkopf R, Kummer FJ, Egol KA. The effect of two different trochanteric nail lag-screw designs on fixation stability of four-part intertrochanteric fractures: a clinical and biomechanical study. J Orthop Sci 2013.
[42] Luo Q, Yuen G, Lau TW, Yeung K, Leung F. A biomechanical study comparing helical blade with screw design for sliding hip fixations of unstable intertrochanteric fractures. ScientificWorldJournal 2013;2013:351936.
[43] Hoffmann S, Paetzold R, Stephan D, Puschel K, Buehren V, Augat P. Biomechanical evaluation of interlocking lag screw design in intramedullary nailing of unstable pertrochanteric fractures. J Orthop Trauma 2013.
[44] Fensky F, Nuchtern JV, Kolb JP, Huber S, Rupprecht M, Jauch SY, Sellenschloh K, Puschel K, Morlock MM, Rueger JM, Lehmann W. Cement augmentation of the proximal femoral nail antirotation for the treatment of osteoporotic pertrochanteric fractures-A biomechanical cadaver study. Injury 2013;44(no. 6):802–7.
[45] Rosenblum SF, Zuckerman JD, Kummer FJ, Tam BS. A biomechanical evaluation of the Gamma nail. J Bone Joint Surg Br 1992;74(3):352–7.